

Generalized Dynamic Predictive Control for Nonlinear Systems Subject to Mismatched Disturbances With Application to PMSM Drives

Xin Dong, *Member, IEEE*, Jianliang Mao , *Member, IEEE*, Yunda Yan , *Member, IEEE*, Chuanlin Zhang , *Senior Member, IEEE*, and Jun Yang , *Fellow, IEEE*

Abstract—This article investigates a generalized dynamic predictive control (GDPC) strategy with a novel autonomous tuning mechanism of the horizon for a class of nonlinear systems subject to mismatched disturbances. As a new incremental function for the predictive control method, the horizon can be determined autonomously with respect to the system working conditions, instead of selecting a fixed value via experience before, which is able to effectively improve the control performance optimization ability to a certain extent considering different system perturbation levels. To this aim, firstly, a nonrecursive composite control framework is constructed based on a series of disturbance observations via higher-order sliding modes. Secondly, by designing a simple one-step scaling gain update mechanism into the receding horizon optimization, the horizon can be therefore adaptively tuned according to its real-time practical operating conditions. A three-order numerical simulation and a typical engineering application of permanent magnet synchronous motor drive system are carried out to demonstrate the effectiveness and conciseness of the proposed GDPC method.

Index Terms—Continuous-time predictive control, mismatched disturbance, permanent magnet synchronous motor (PMSM), robustness and adaptiveness balance, self-tuning receding horizon.

Manuscript received 19 October 2022; revised 5 January 2023; accepted 7 February 2023. Date of publication 22 February 2023; date of current version 10 July 2023. This work was supported in part by the National Natural Science Foundation of China under Grant 62173221 and Grant 62203292, in part by the Jiangsu Province Industry-University-Research Collaboration Project under Grant BY2021304, and in part by the U.K. Engineering and Physical Science Research Council (EPSRC) New Investigator Award under Grant EP/W027283/1. (*Corresponding author: Chuanlin Zhang*)

Xin Dong, Jianliang Mao, and Chuanlin Zhang are with the College of Automation Engineering, Shanghai University of Electric Power, Shanghai 200090, China (e-mail: xxddong@shiep.edu.cn; jl_mao@shiep.edu.cn; clzhang@shiep.edu.cn).

Yunda Yan is with the School of Engineering and Sustainable Development, De Montfort University, Leicester LE1 9BH, U.K. (e-mail: yd.yan@ieee.org).

Jun Yang is with the College of Aeronautical and Automotive Engineering, Loughborough University, Loughborough LE11 3TU, U.K. (e-mail: j.yang3@lboro.ac.uk).

Color versions of one or more figures in this article are available at <https://doi.org/10.1109/TIE.2023.3245213>.

Digital Object Identifier 10.1109/TIE.2023.3245213

I. INTRODUCTION

MODEL predictive control (MPC) is regarded as a promising control strategy that has attracted a great deal of attention from industrial practitioners, owing to its implementation simplicity and high-performance trajectory regulation [1], [2], [3]. Notably, with the development of semiconductor science and microprocessors, the constrained application range of MPC has been extended from slow time-varying systems to fast dynamic systems, e.g., power converters [4], [5], multiple robots control [6], PMSM [7], [8], [9], etc.

Facing such a large application prospect, the requirements for higher precision and faster response are continuously increasing in industrial systems recently, which brings more challenges to the design of MPC approaches. An inevitable problem is that the existing disturbances certainly result in undesirable impacts on the closed-loop control performance for the baseline MPC framework. Moreover, when encountering time-varying mismatched disturbance, the response precision and dynamic performance are more difficult to guarantee [10].

Actually, disturbance rejection is one of the most important issues in control systems. In the early years, the conventional robust control was developed to suppress the disturbance negative impacts, see e.g., [7], [11], etc. Nonetheless, the fact deserved to be emphasized is that this manner tends to render the asymptotic result and restrain disturbance asymptotically via feedback regulation in a relatively slow way, rather than handle the disturbances directly by controller design [12]. For pursuing higher precision, the disturbance/uncertainty estimation and attenuation (DUEA) scheme receives more and more attention from practitioners, see e.g., [10], [13], [14], etc. This approach category is greatly developed by industry scholars and applied properly in many control application fields, such as various vehicles control [15], [16] and aircraft control [17]. By integrating with feedback compensation technology, the built composite approaches have been proven promising to attenuate the undesirable effect brought by perturbation [18], [19].

Since the active intervention strategy is the potential to cope with the disturbance and uncertainty issues in industrial application scenarios, a natural thought is that one can integrate the DUEA design into the baseline MPC scheme aiming to improve

the control precision. Indeed, there are many existing related theoretical and practical works that have been investigated. For example, the trajectory of the nonlinear tracking system subject to matched/mismatched disturbances and input constraints were be regulated by a reduced order disturbance-observer-based fuzzy MPC in [20]. The authors in [21] investigated an observer-based robust tracking predictive controller for discrete-time nonlinear affine systems to cope with changing setpoints and nonadditive nonslowly varying unknown disturbance with bounded variations. A composite controller constituted by an explicit nonlinear MPC and a nonlinear disturbance observer (NDO) is proposed to tackle the autonomous flight of small-scale helicopters, which can be referred to [22]. One can also refer to [23], [24], and references therein, etc.

Whereas, after partially revisiting the above, it is notable that the MPC integrated with disturbance rejection results are mostly based on the fixed horizon design. With the presence of time-varying mismatched disturbance, the fixed horizon, determined upon human experience, can ensure robustness to a certain extent. However, considering the case when mismatched disturbance varies within a large range, the selected horizon may be too conservative for wide working conditions, and therefore, one direct problem is that the transient-time control performance will be possibly deteriorated, i.e., the control optimization ability is limited in such cases and clearly a tunable predictive period matters under complicated and frequent changing working conditions.

For ease of understanding, the electric vehicle control scenarios are taken as an example. On one hand, on relatively smooth ground, the output speed should have a fast response ability while ensuring a comfortable ride experience for passengers, which corresponds to the internal PMSM controller regulation performance. With the conventional generalized predictive control (GPC) approaches [25], [26], the fixed horizon would be mainly suitable for a unique working condition. Once the desired value of the speed changes, a larger horizon may give rise to a bumpy experience for passengers, i.e., possible response overshoot. On the other hand, for special driving conditions such as uphill and road bumps, the steady-state speed will not change drastically, which also leads to a challenge for the onboard motor. Accordingly, the dynamic horizon design manner seems to be more feasible in practical implementations with complex operating conditions.

Consequently, aiming to present a partial solution to the aforementioned problems, a novel generalized dynamic predictive control (GDPC) strategy is established. Firstly, a higher-order sliding mode disturbance observer is applied to reconstruct the internal matched/mismatched disturbances, and the compensating loop is subsequently designed. On this occasion, an equivalent nominal system is obtained. Secondly, by ignoring the estimation errors, one can derive the implementable nominal chain of integrators, and consequently, the traditional nonlinear GPC law yields. At last, motivated by the dynamic scaling gain design in references [27] and [28], a horizon online updating mechanism is built aiming to enhance the suitability of the

conventional GPC when facing disturbance fluctuations. Compared with the existing results, this article is mainly dedicated to making improvements in the following areas.

- 1) The offline MPC and online updating horizon mechanism are integrated into the proposed GDPC framework, which not only reduces the computational burdens, but also endows the control system with adaptive transient-time performance optimization capabilities facing working condition fluctuations.
- 2) An offset-free predictive controller is built by employing a composite nonrecursive synthesis manner under a semiglobal control framework, therefore both the predictive controller form and adaptive update mechanism are largely simplified, which facilitates the implementation in industrial applications.

The rest of this article is organized as follows. The primary theoretical results are placed in Sections II and III. Sections IV and V verify the efficacy of the proposed controller from the points of a three-order numerical simulation and a series of real-life experiments applied to PMSM drive control. Finally, Section VI concludes this article. The main stability analysis is provided in the Appendix.

II. PROBLEM STATEMENTS

This article constructs a GDPC design framework to deal with the trajectory regulation problem for the following candidate nonlinear system:

$$\begin{cases} \dot{x}_i = x_{i+1} + f_i(\bar{x}_i) + d_i, & i = 1, 2, \dots, n-1 \\ \dot{x}_n = u + f_n(x) + d_n \\ y = x_1 \end{cases} \quad (1)$$

where $\bar{x}_i = (x_1, x_2, \dots, x_i)^\top$, $x = \bar{x}_n$, u , and y are the system partial state vector, full state vector, control input, and output, respectively. $d_i, i = 1, 2, \dots, n$ is regarded as a bounded disturbance term. $f_i(\cdot), i = 1, 2, \dots, n$ is a known smooth nonlinear function. Meanwhile, the initial time is denoted as $t_0 = 0$ while the initial state vector is denoted by x_0 . y_r is denoted as the tracking reference signal.

The control objective of this article is to develop a composite controller to grant the control system the antidisturbance ability while achieving an asymptotic regulation result, i.e., $\lim_{t \rightarrow \infty} y = y_r$, and the tracking error is defined as $e_s = y - y_r$.

The following assumptions, which are quite reasonable in practice, are essential for theoretical deductions thereafter.

Assumption 1: The reference signal y_r and its n th order derivative are piecewise continuous, known, and bounded.

Assumption 2: The disturbance $d_i, i = 1, 2, \dots, n$ and its $n-i+1$ order derivatives are assumed to be bounded.

III. MAIN THEORETICAL RESULTS

In this section, the details of the controller construction procedure are presented in an explicit manner.

A. System Performance Recovery and Pre-Treatment

To proceed, a higher-order sliding mode observer (HOSMO) is constructed, in order to achieve rapid system performance recovery. By defining that $\beta_{i,j} = \frac{1}{n+2-i-j}$, $\zeta_{i,j} = z_{i,j} - \nu_{i,j}$, and the design parameters $\alpha_{i,j} > 0$, $l_i > 0$ with $i = 1, 2, \dots, n$, $j = 0, 1, \dots, n-i+1$, the expressions of HOSMO are depicted as the following form [30]:

$$\begin{aligned}\dot{z}_{i,0} &= \nu_{i,1} + x_{i+1} + f_i(\bar{x}_i), \quad i = 1, 2, \dots, n \\ \dot{z}_{i,1} &= \nu_{i,2}, \dots, \dot{z}_{i,k} = \nu_{i,k+1}, \quad k = 1, 2, \dots, n-i+1\end{aligned}\quad (2)$$

where $|w|^r \triangleq \text{sign}(w)|w|^r$, $\forall r \geq 0$

$$\begin{aligned}\nu_{i,0} &= x_i, \quad \nu_{i,1} = -\alpha_{i,0} l_i^{\beta_{i,0}} [\zeta_{i,0}]^{1-\beta_{i,0}} + z_{i,1} \\ \nu_{i,j+1} &= -\alpha_{i,j} l_i^{\beta_{i,j}} [\zeta_{i,j}]^{1-\beta_{i,j}} + z_{i,j+1} \\ \nu_{i,n-i+2} &= -\alpha_{i,n-i+1} l_i^{\beta_{i,n-i+1}} [\zeta_{i,n-i+1}]^{1-\beta_{i,n-i+1}}\end{aligned}$$

are regarded as the auxiliary states in the observer system for $i = 1, 2, \dots, n$, $j = 1, 2, \dots, n-i$; $x_{n+1} = u$; $z_{i,0} = \hat{x}_i$, $z_{i,1} = \hat{d}_i$, and $z_{i,j} = \hat{d}_i^{(j-1)}$ are estimations of x_i , d_i , and $d_i^{(j-1)}$, respectively.

Remark 1: The utilized observer (2) will promisingly reconstruct the unknown disturbance signals within a finite time. The selection guideline of the observer gain l_i tends to be appropriately large aiming to estimate the disturbances accurately. Meanwhile, for the purpose of achieving desirable disturbance estimation performance, $\alpha_{i,j}$ can be selected in a “trial and error” manner according to the current output response.

At this point, by employing an auxiliary variable $\chi_i(d, \bar{y}_r)$ with $d \triangleq (d_1, d_1^{(1)}, \dots, d_i^{(n)}, \dots, d_{n-1}, d_{n-1}^{(1)}, d_n)^\top$ and $\bar{y}_r \triangleq (y_r, y_r^{(1)}, \dots, y_r^{(n)})^\top$, depicted as the following equations, the steady-state reference functions are able to be constructed:

$$\begin{aligned}\chi_1 &= y_r \\ \chi_i &= \frac{d\chi_{i-1}}{dt} - f_{i-1}(\bar{x}_{i-1}) - d_{i-1}, \quad i = 2, 3, \dots, n+1\end{aligned}\quad (3)$$

where $\bar{x}_i = (\chi_1, \chi_2, \dots, \chi_i)^\top$, $i = 1, 2, \dots, n+1$.

Combining with (2), one is able to modify the series of implementable steady-state reference functions by substituting $\frac{\partial d_j}{\partial t^j}$ with $\zeta_{i,j+2}$, detailedly, and they can be expressed as the following form by denoting $z = (z_{1,0}, z_{1,1}, \dots, z_{1,n}, \dots, z_{n,1})^\top$:

$$\begin{cases} x_1^{\text{ref}} = \chi_1 = y_r \\ x_i^{\text{ref}} = \chi_i(z, \bar{y}_r), \quad i = 2, 3, \dots, n+1. \end{cases}\quad (4)$$

To proceed, a natural procedure is to implement the state-space model transformation given as

$$\begin{cases} \eta_i = x_i - x_i^{\text{ref}}, \quad i = 1, 2, \dots, n \\ v = u - x_{n+1}^{\text{ref}}. \end{cases}\quad (5)$$

By this means, the following equivalent stabilizable system can be derived:

$$\begin{cases} \dot{\eta}_i = \eta_{i+1} + f_i(\bar{x}_i) - f_i(\bar{x}_i^{\text{ref}}) + \varepsilon_i, \quad i = 1, \dots, n-1 \\ \dot{\eta}_n = v + f_n(x) - f_n(x^{\text{ref}}) + \varepsilon_n \end{cases}\quad (6)$$

in which $\bar{x}_i^{\text{ref}} = (x_1^{\text{ref}}, x_2^{\text{ref}}, \dots, x_i^{\text{ref}})^\top$, $x^{\text{ref}} = \bar{x}_n^{\text{ref}}$, $\varepsilon_i = f_i(\bar{x}_i^{\text{ref}}) + x_{i+1}^{\text{ref}} - \dot{x}_i^{\text{ref}} - (f_i(\bar{x}_i) + \chi_{i+1} - \dot{\chi}_i)$, and $i = 1, 2, \dots, n$.

B. Receding-Horizon Optimization

To begin with, a simple receding-horizon performance index is provided to regulate the output of the system (1) to optimally converge to the reference signal [31]

$$J(t) = \frac{1}{2} \int_0^T e_s^2(t+\tau) d\tau \quad (7)$$

where $T > 0$ is the horizon.

In what follows, the nominal system (6) can be concisely depicted as the compact form by ignoring the estimation errors

$$\dot{\eta} = A\eta + Bu \quad (8)$$

where $\eta = [\eta_1, \eta_2, \dots, \eta_n]^\top$ and (A, B) are matrices in the controllable canonical form. Then, the tracking error $e_s(t+\tau)$ within a horizon (i.e., $0 \leq \tau \leq T$) can be predicted by Taylor series expansion given as the following along system (8):

$$\begin{aligned}\hat{e}_s(t+\tau)|_{(8)} &\doteq \eta_1 + \tau\eta_2 + \dots + \frac{\tau^{n-1}}{(n-1)!}\eta_n + \\ &\quad \frac{\tau^n}{n!}v + \dots + \frac{\tau^{n+r}}{(n+r)!}v^{(r)} = \bar{\mathcal{H}}\eta + \tilde{\mathcal{H}}V\end{aligned}\quad (9)$$

where $\bar{\mathcal{H}} \triangleq \left[1, \tau, \dots, \frac{\tau^{n-1}}{(n-1)!}\right]^\top$, $\tilde{\mathcal{H}} \triangleq \left[\frac{\tau^n}{n!}, \frac{\tau^{n+1}}{(n+1)!}, \dots, \frac{\tau^{n+r}}{(n+r)!}\right]^\top$, $V \triangleq [v, v^{(1)}, \dots, v^{(r)}]^\top$, and r is the control order [2].

Subsequently, combined with (9), the performance index defined by (7) can be calculated specifically as

$$\begin{aligned}\hat{J}(t) &\triangleq \frac{1}{2} \int_0^T \hat{e}_s^2(t+\tau) d\tau \\ &= \frac{1}{2} \eta^\top \mathcal{H}_1 \eta + \eta^\top \mathcal{H}_2 V + \frac{1}{2} V^\top \mathcal{H}_3 V\end{aligned}\quad (10)$$

where $\mathcal{H}_1 \triangleq \int_0^T \bar{\mathcal{H}}^\top \bar{\mathcal{H}} d\tau \in \mathbb{R}^{n \times n}$, $\mathcal{H}_2 \triangleq \int_0^T \bar{\mathcal{H}}^\top \tilde{\mathcal{H}} d\tau \in \mathbb{R}^{n \times (r+1)}$, and $\mathcal{H}_3 \triangleq \int_0^T \tilde{\mathcal{H}}^\top \tilde{\mathcal{H}} d\tau \in \mathbb{R}^{(r+1) \times (r+1)}$.

Taking partial derivative of $\hat{J}(t)$ with respect to V , it can be depicted as $\partial \hat{J} / \partial V = \mathcal{H}_2^\top \eta + \mathcal{H}_3 V$. It is clear that the matrix \mathcal{H}_3 is positive definite. By setting $\partial \hat{J} / \partial V = 0$ and $\partial^2 \hat{J} / \partial V^2 > 0$, the optimal controller is obtained as $V^* = -\mathcal{H}_3^{-1} \mathcal{H}_2^\top \eta$. Then, the implementable optimal intermediate law is developed as

$$v^* = -\mathcal{B} \mathcal{H}_3^{-1} \mathcal{H}_2^\top \eta \quad (11)$$

where $\mathcal{B} \triangleq [1, 0, \dots, 0] \in \mathbb{R}^{r+1}$. Taking $\mathcal{H}_2(i, j) = p_{i,j} T^{n+i+j-1}$ and $\mathcal{H}_3(i, j) = q_{i,j} T^{2n+i+j-1}$ into consideration, the optimal intermediate controller can be simplified as $v^* = -\frac{k_1^*}{T^n} \eta_1 - \frac{k_2^*}{T^{n-1}} \eta_2 - \dots - \frac{k_n^*}{T} \eta_n$, where $p_{i,j}$, $q_{i,j}$, and k_i^* are constants related to r and n . Noting that the above derivations still hold when the receding horizon is variable or state-related, therefore the optimal controller can be expressed as

$$u^* = -\frac{k_1^*}{T^n} \eta_1 - \frac{k_2^*}{T^{n-1}} \eta_2 - \dots - \frac{k_n^*}{T} \eta_n + x_{n+1}^{\text{ref}}. \quad (12)$$

At this stage, it is common that the horizon of the traditional GPC is generally selected as a fixed value at (12), which relies

on engineers' experiences. However, the fixed horizon predictive control may possibly lead to variability in performance optimization under various working conditions. In practice, as motivated in the introduction, a variable horizon mechanism with respect to different working conditions would present a more reliable control result regarding the GPC design. In the subsequent section, we are aiming to design a novel and simple horizon tuning mechanism for the optimal controller (12).

C. Self-Tuning Mechanism for the Horizon

Denote $K \triangleq \left[\frac{k_1^*}{T_0^n}, \frac{k_2^*}{T_0^{n-1}}, \dots, \frac{k_n^*}{T_0} \right]$ which is viewed as the control gain vector of the optimal controller and T_0 is the initial value of horizon, $\Theta = \text{diag}\{0, 1, \dots, n-1\}$. Then, there exists a matrix $Q \in \mathbb{R}^{n \times n}$ subject to $Q = Q^\top > 0$, such that $(A - BK)^\top Q + Q(A - BK) \leq -I_n$, where I_n is the n th order identity matrix. Additionally, ϱ is a positive design parameter determined by

$$\varrho > \max \left\{ 0, -\frac{\lambda_{\min}(\Theta Q + Q\Theta)}{2\lambda_{\min}(Q)} \right\} \quad (13)$$

where $\lambda_{\max}(\cdot)$ and $\lambda_{\min}(\cdot)$ are the maximum and the minimum eigenvalues of the matrix (\cdot) , respectively.

Aiming to design an autonomous tuning mechanism for the dynamic horizon, with the rescaled transformation $\xi_i = \eta_i/L^{\varrho+i-1}$, $i = 1, 2, \dots, n$, $\xi \triangleq [\xi_1, \xi_2, \dots, \xi_n]^\top$, and $\|\xi\| \triangleq \sqrt{\xi^\top \xi}$, we introduce the following adaption law to grant T the self-configuration ability:

$$\begin{cases} T = T(0)/L, T(0) > 0 \\ \dot{L} = c\|\xi\|^2, L(0) = 1 \end{cases} \quad (14)$$

where L is an auxiliary scaling gain function and $c > 0$ is a design parameter to restrain the growth rate of L .

Theorem 3.1: For a nonlinear system (1) under the disturbance observer (2) and the optimal control action (12) with a self-tuning horizon (14), provided that the initial value of system states satisfy $x_0 \in [-\rho, \rho]^n$ with ρ being an arbitrarily large positive constant, the following statements hold.

- 1) All signals in the closed-loop system (1)–(2)–(12) are uniformly bounded.
- 2) $\lim_{t \rightarrow \infty} y = y_r$.

The control diagram of the proposed controller can be depicted in Fig. 1. Meanwhile, for the sake of the readability of this article, the laborious semiglobal stability analysis is listed in the Appendix.

Remark 2: During the controller design process, the basic parameter selection criteria can be specifically listed as the following steps.

- 1) The optimal control gains k_i^* is calculated by (10).
- 2) After solving joint linear matrix inequalities, the matrix feasible solution of Q can be obtained.
- 3) The design parameter ϱ is determined by calculating a simple linear inequality shown in (13), which commonly can be selected as a small positive value, and even can be zero in application-oriented scenarios.
- 4) The scaling gain c linked to the convergence of T is generally chosen via the “trial and error” method.

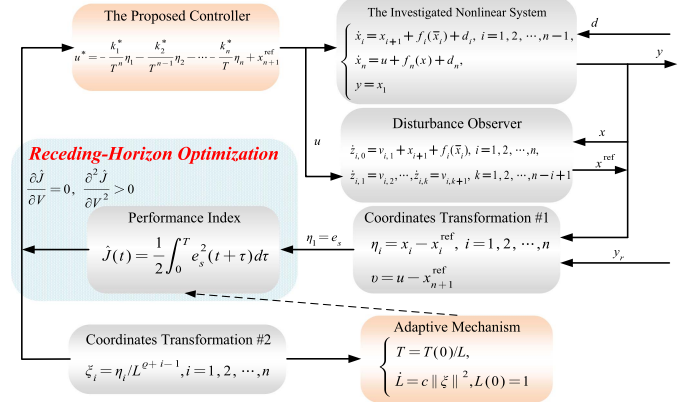


Fig. 1. Control diagram of the proposed strategy.

- 5) T_0 is the key parameter in this approach, which is selected according to the error between the real-time output response and expectations.

IV. NUMERICAL SIMULATION TESTS

In this section, an illustrative three-order nonlinear system subject to mismatched and matched disturbances is presented to illustrate the efficacy of the proposed control method, which is denoted as the following form:

$$\begin{cases} \dot{x}_1 = x_2 + \sin(x_1 + \frac{\pi}{3}) + d_1 \\ \dot{x}_2 = x_3 + x_1 x_2^{4/3} + d_2 \\ \dot{x}_3 = u + \ln(1 + x_2^2) + d_3 \end{cases} \quad (15)$$

where $d_1 = \sin(t) + \cos(t)$ is the mismatched disturbance and $d_2 = 1.2$ is the matched disturbance, while the reference signal $y_r = -0.3 + e^{-t}$, $t \in [0, \infty)$.

According to the proposed control design procedure, the first step is to build a HOSMO to estimate exactly d_1 , d_2 , and their corresponding derivatives, i.e., $z_{1,1}$, $z_{1,2}$, $z_{1,3}$, and $z_{2,1}$. Consequently, we are capable of constructing the implementable steady-state reference functions: $x_1^{\text{ref}} = y_r$, $x_2^{\text{ref}} = \dot{y}_r - \sin(y_r + \frac{\pi}{3}) - z_{1,1}$, $x_3^{\text{ref}} = y_r^{(2)} - \cos(y_r + \frac{\pi}{3}) \dot{y}_r - z_{1,2} - y_r (x_2^{\text{ref}})^{4/3}$, and $x_4^{\text{ref}} = y_r^{(3)} + \sin(y_r + \frac{\pi}{3}) y_r^2 - \cos(y_r + \frac{\pi}{3}) y_r^{(2)} - z_{1,3} - \dot{y}_r (x_2^{\text{ref}})^{4/3} - \frac{4}{3} y_r (x_2^{\text{ref}})^{1/3} (y_r^{(2)} - \cos(y_r + \frac{\pi}{3}) \dot{y}_r - z_{1,2}) - \ln(1 + (x_2^{\text{ref}})^2) - z_{2,1}$. Thereafter, the coordinate transformations are depicted as $\eta_1 = x_1 - x_1^{\text{ref}}$, $\eta_2 = x_2 - x_2^{\text{ref}}$, $\eta_3 = x_3 - x_3^{\text{ref}}$, and $v = u - x_4^{\text{ref}}$.

With the preparation of the preliminary work, one could structure the optimal regulation law straightforwardly as the following form, and for simplicity, r is set as 0:

$$\begin{cases} u = -\left(\frac{k_1^*}{T^3} \eta_1 + \frac{k_2^*}{T^2} \eta_2 + \frac{k_3^*}{T} \eta_3\right) + x_4^{\text{ref}} \\ T = T(0)/L, L(0) = 1 \\ \dot{L} = c \left(\frac{\eta_1^2}{L^{2\varrho}} + \frac{\eta_2^2}{L^{2\varrho+2}} + \frac{\eta_3^2}{L^{2\varrho+4}}\right). \end{cases}$$

From another perspective, for the purpose of showing the concision of the proposed controller law form, the dynamic surface control (DSC) strategy integrated with the NDO is utilized [32], [33], which is commonly regarded as an effective methodology

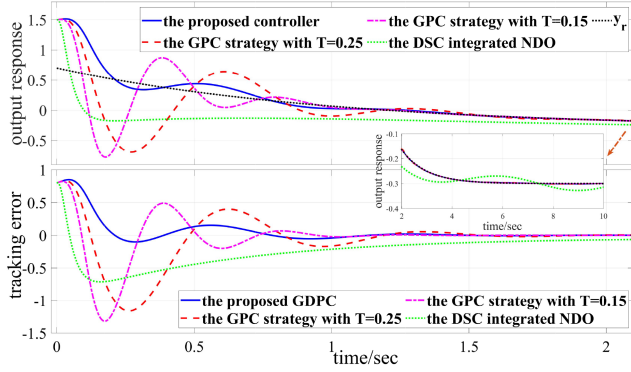
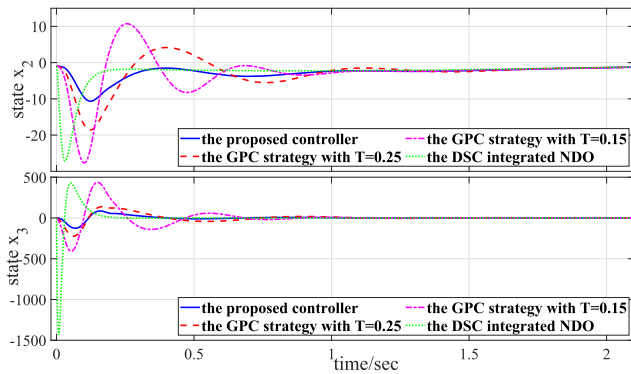


Fig. 2. Response curves of the output and tracking errors.

Fig. 3. Response curves of system states x_2 and x_3 .

to mitigate recursive strategy complexity explosion. Specifically, the composite candidate controller can be expressed as

$$\begin{aligned} \hat{d}_1 &= \kappa_1(x_1 - p_1) & \hat{d}_2 &= \kappa_2(x_3 - p_2) \\ \dot{p}_1 &= x_2 + \sin\left(x_1 + \frac{\pi}{3}\right) + \hat{d}_1 & \dot{p}_2 &= u + \ln(1+x_2^2) + \hat{d}_2 \end{aligned}$$

$$\begin{cases} S_1 = x_1 - y_r, \quad S_2 = x_2 - x_{2d}, \quad S_3 = x_3 - x_{3d} \\ \varpi_1 \dot{x}_{2d} + x_{2d} = -\lambda_1 S_1 - \sin\left(x_1 + \frac{\pi}{3}\right) - \hat{d}_1 + \dot{x}_1 \\ \varpi_2 \dot{x}_{3d} + x_{3d} = -\lambda_2 S_2 - x_1 x_2^{4/3} + \dot{x}_2 \\ u = -\lambda_3 S_3 - \ln(1+x_2^2) - \hat{d}_2 + \dot{x}_3 \end{cases}$$

where $\kappa_i > 0$, $\lambda_j > 0$, $\varpi_i > 0$, $i = 1, 2$, and $j = 1, 2, 3$ are the control gains, the filter time constants of first-order filters.

To proceed, the initial values are given as $T_0 = 0.8$; $x_0^\top = [1.5, -1, 0]$; $z^\top(0) = 0$; $x_{2d}(0) = x_{3d}(0) = 0$. The control gains can be calculated as $[k_1^*, k_2^*, k_3^*] = [\frac{21}{2}, \frac{42}{5}, \frac{7}{2}]$ via (10). Besides, the parameters of HOSMO are selected as $[\alpha_{1,0}, \alpha_{1,1}, \alpha_{1,2}, \alpha_{1,3}, l_1; \alpha_{3,0}, \alpha_{3,1}, l_3] = [12, 18, 24, 24, 120; 28, 56, 80]$, and the design parameters are $[c, \varrho] = [0.01, 0.01]$. Additionally, the control gains of the composite candidate controller are $[\kappa_1, \kappa_2] = [28, 40]$; $[\lambda_1, \lambda_2, \lambda_3] = [2.4, 1.5, 1.5]$; $[\varpi_1, \varpi_2] = [0.01, 0.01]$. The fixed horizon of the conventional GPC in (12) is selected as 0.15 and 0.25, as the control group. The control result figures are shown in Figs. 2–4.

Subsequently, analyzing one by one, one can observe in Fig. 2 that the control objective is basically achieved via all

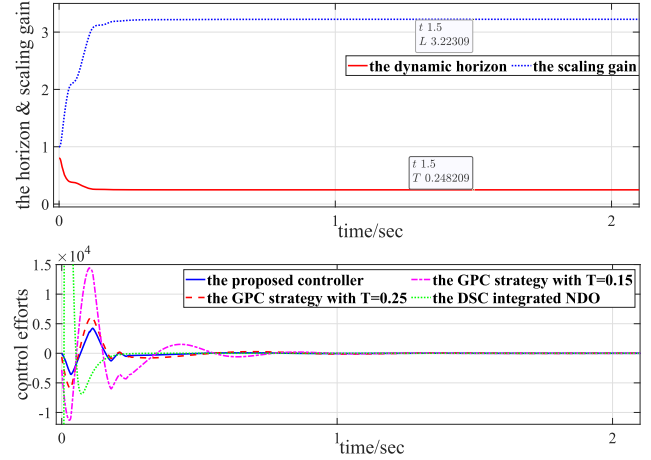


Fig. 4. Dynamic horizon response and control efforts.

TABLE I
PERFORMANCE INDEXES OF SIMULATION RESULTS

Controllers	ISE	MSE
The proposed controller	84.770	0.041
The GPC strategy with $T = 0.15$	241.966	0.121
The GPC strategy with $T = 0.25$	319.138	0.159
The DSC integrated NDO	235.941	0.118

the candidate controllers. One interesting fact is that the horizon plays a key role in the intensity of the response curve listed in Fig. 2, and furthermore, the response curve of the proposed controller is more satisfactory compared with the other controllers, which implies that the internal robustness redundancy is possibly released to some extent. The dynamic horizon converges from the initial value to 0.248. From another perspective, in Fig. 4, the control consumption of the proposed controller is clearly lower than other controllers, and the optimized recursive strategy consumes the most. The detailed performance indexes are listed in Table I.

V. EXPERIMENTAL VERIFICATION OF A PMSM DRIVE SYSTEM

In this section, a typical application of a PMSM drive system is implemented to validate the efficacy of the proposed GDPC algorithm.

A. Model Description and Controller Design

Firstly, the dynamic model of a surface-mounted PMSM in the d - q frame is formulated as [34]

$$\begin{cases} \dot{\omega} = \frac{1}{J} \left(\frac{3}{2} n_p \psi_f i_q - B\omega - T_L \right) \\ \dot{i}_d = \frac{1}{L_s} (-R_s i_d + n_p \omega L_s i_q + u_d) \\ \dot{i}_q = \frac{1}{L_s} (-R_s i_q - n_p \omega L_s i_d - n_p \psi_f \omega + u_q) \end{cases} \quad (16)$$

where u_d , u_q , i_d , and i_q are the stator voltages and currents of the d - and q -axes, respectively, ω is the angular velocity, n_p is the number of pole pairs, R_s is the stator resistance, L_s is the stator inductance, ψ_f is the rotor flux linkage, T_L is the load torque, J is the rotor inertia, and B is the viscous frictional coefficient. Besides, the reference rotating speed is defined as ω_{ref} in this article. For system (16), consider an ideal

tracking case for d -axis current, i.e., $i_d \dot{=} i_d^* = 0$. Furthermore, we introduce the following transformation $x_1 = \omega_{\text{ref}} - \omega$, $x_2 = (-\frac{3}{2}n_p\psi_f i_q + B\omega_{\text{ref}})/J$, which are regarded as the system states. Specifically, the control-oriented model is rewritten as

$$\begin{cases} \dot{x}_1 = x_2 - Bx_1/J + d_1, \quad y = x_1 \\ \dot{x}_2 = u - \frac{3}{2}\left(n_p^2\psi_f^2x_1 - (n_p^2\psi_f^2 + \frac{2}{3}R_sB)\omega_{\text{ref}}\right)/(JL_s) \\ \quad - R_s x_2/L_s + d_2 \end{cases}$$

where $u = -1.5n_p\psi_f u_q/(JL_s)$ is the control input, y is the system output, and $d_1 = T_L/J$ is viewed as the mismatched disturbance and d_2 is the matched disturbance which contains unmodeled dynamic or measurement errors, etc.

At this point, we have transferred the rotating speed regulation problem into a stabilizable one. By the proposed means, one can calculate the steady-state functions as $x_1^{\text{ref}} = 0$, $x_2^{\text{ref}} = -z_{1,1}$, and $x_3^{\text{ref}} = -z_{1,2} - \frac{1}{JL_s}(R_s J z_{1,1} + (\frac{3}{2}n_p^2\psi_f^2 + R_s B)\omega_{\text{ref}}) - z_{2,1}$, where $z_{1,1}$, $z_{1,2}$, and $z_{2,1}$ are derived from (2). Hence, the coordinate transformations are $\eta_1 = x_1 - x_1^{\text{ref}}$, $\eta_2 = x_2 - x_2^{\text{ref}}$, and $v = u - x_3^{\text{ref}}$. Then, one is able to formulate the controller in the following form utilizing the proposed framework:

$$\begin{aligned} u &= -\left(\frac{k_1^*}{T^2}\eta_1 + \frac{k_2^*}{T}\eta_2\right) + x_3^{\text{ref}}, \quad T = T_0/L \\ \dot{L} &= c\left(\frac{\eta_1^2}{L^{2\varrho}} + \frac{\eta_2^2}{L^{2\varrho+2}}\right)(1 + \text{sign}(|e_s| - \delta)), \quad L(0) = 1 \end{aligned} \quad (17)$$

where $\delta > 0$ is an arbitrarily small tolerance, commonly can be set as slightly larger than the system tolerance value.

It is noted that in (17), a threshold is added to the adaption law. When $|e_s| \leq \delta$, it is clear that T will converge to a certain constant. The reason is that in practical implementations, by acknowledging the measurement noises and inevitable system uncertainties, the output tracking error is impossible to converge to zero, which renders an uncontrollable decrease of T , and departs from control expectations.

B. Simulations-Parameters Configuration

For the purpose of validating the influence of the design parameters upon the output speed and the horizon convergence, here we implement several simple simulations first that facilitate the parameter selection for the following experiments.

To begin with, the simulation scenario should be clarified that: *The reference output speed is constant at 500 r/min for $t \in [0, 1]$, at 1000 r/min for $t \in (1, 2]$, with no load. Thereafter at 1.5 s, the 30% nominal torque load (0.0817 Nm) is considered.*

Specifically, Fig. 5 describes the role of the T_0 value in the output channel and the dynamic horizon. One can find that a larger T_0 leads to a slower, but more smooth, speedy recovery process. With the increase of T_0 , the settling time reduces. However, when T_0 is smaller than 0.8, the possible robustness redundancy occurs, and the recovery process becomes more intense that it has a certain overshoot. From this perspective, T_0 is a vital parameter to deserve to be carefully chosen, which

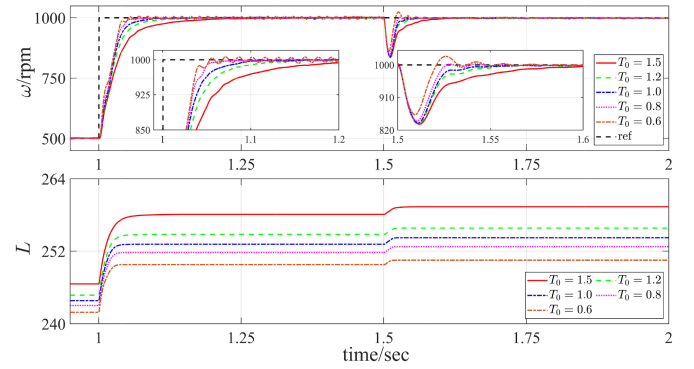


Fig. 5. Influence upon the output speed and the dynamic scaling gain L convergence of the parameter T_0 .

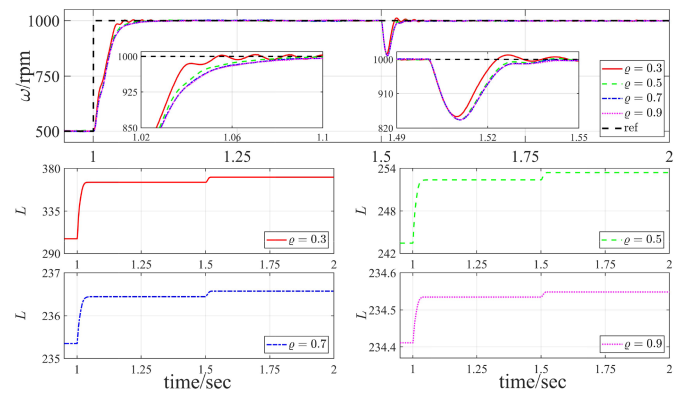


Fig. 6. Influence upon the output speed and the dynamic scaling gain L convergence of the parameter ϱ .

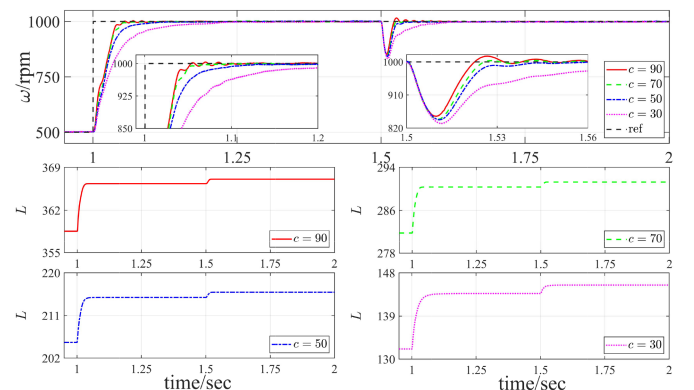


Fig. 7. Influence upon the output speed and the dynamic scaling gain L convergence of the parameter c .

can be selected as near 1 in the speed regulation of the PMSM drive.

In Figs. 6 and 7, the parameters ϱ and c are analyzed, respectively. Here, we present them together because they are the scaling gains, which have a similar influence on the output speed and the convergence of the dynamic horizon. Detailedly, in Fig. 6, one can get that clearly, the smaller the ϱ is, the bigger the L is, corresponding to the smaller T , which results in the more

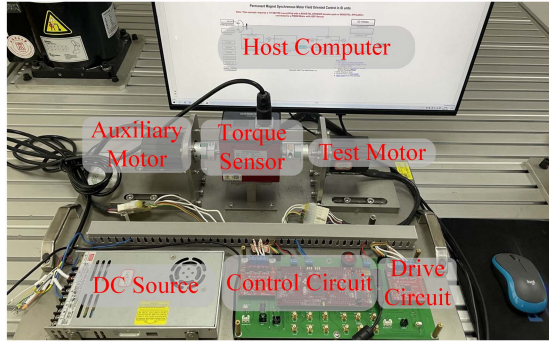


Fig. 8. Experimental setup.

TABLE II
PARAMETERS OF THE PMSM DRIVE SYSTEM

Parameter description (symbol)	Value
Number of pole pairs (n_p)	4
Stator resistance (R_s)	0.36Ω
Stator inductance (L_s)	2×10^{-4} mH
Rotor flux linkage (ψ_f)	0.0064Wb
Rotor inertia (J)	7.066×10^{-6} kg·m ²
Viscous frictional coefficient (B)	2.637×10^{-6} N·m·s/rad
Rated current (I_N)	7.1A
Switching frequency (f_{sw})	15kHz
Observer #1 gains ($(l_1, \alpha_{1,1}, \alpha_{1,2}, \alpha_{1,3})$)	1200, 40, 48, 54
Observer #2 gains ($(l_2, \alpha_{2,1}, \alpha_{2,2})$)	1×10^7 , 72, 84
Controller gains ((k_1^*, k_2^*))	10/3, 2.5
Design parameters ($(T_0, \varrho, c, \delta)$)	1s, 1, 0.5, 15
Fixed-horizon of GPC approach (T)	5ms
PI gains of i_d -axis ((k_{dp}, k_{di}))	2.3197, 0.2817
PI gains of i_q -axis ((k_{pp}, k_{pi}))	$2, 6.6675 \times 10^{-4}$

drastic regulation process. If ϱ is set as a relatively large value, the process is smooth, and the settling time becomes longer. On the other hand, the influence of c is inversely similar.

C. Experiment Verification

1) Experimental Setup: The experimental configuration, depicted in Fig. 8, in the laboratory is made up of a control circuit in the platform TI LAUNCHXL-F28379D with the switching frequency of 15 kHz, a drive circuit BOOSTXLDVR8305EVM, a torque sensor with a range of 0–1 Nm, a test motor, and an auxiliary loading motor. Besides, the parameters of the PMSM platform are listed in Table II.

2) Experiment Results: The experiments are carried out from two perspectives. On one hand, in addition to the proposed GDPC approach, the other two existing control methodologies are chosen to compare the control performance, i.e., the traditional double-loop PI control and the GPC control with a fixed horizon. On the other hand, the speed regulation conditions of the PMSM are essential to be rigorously designed. Concretely, the test experiments are conducted from the following three scenarios.

Scenario 1. The reference speed switches from 500 r/min to 1500 r/min with $T_L = 0.02$ Nm: The experiment results of this case can be referred to in Fig. 9. In this case, the worst speed response is clearly the PI controller, whether settling

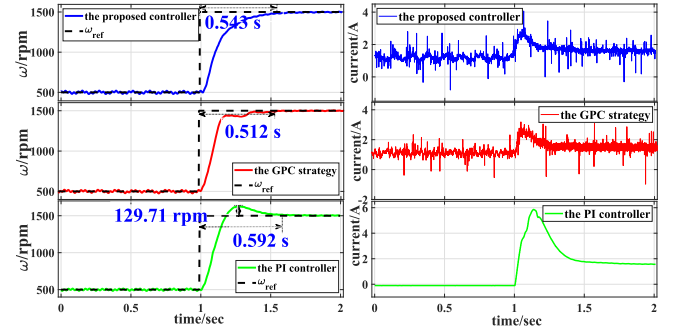


Fig. 9. Experiment results of the reference speed switches from 500 r/min to 1500 r/min with $T_L = 0.02$ Nm.

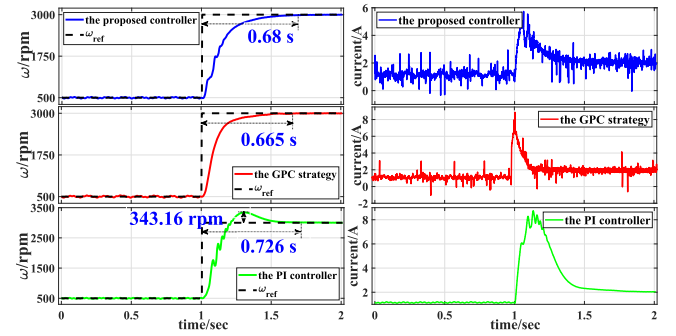


Fig. 10. Experiment results of the reference speed switches from 500 r/min to 3000 r/min with $T_L = 0.02$ Nm.

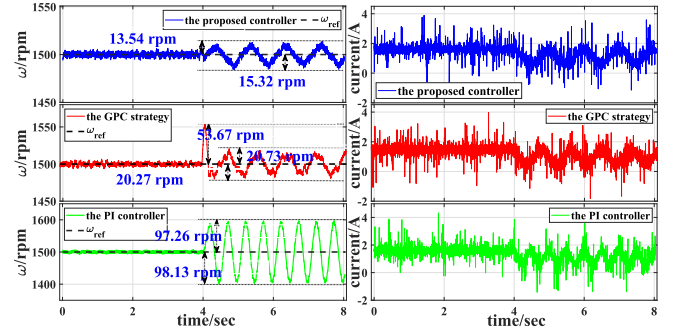


Fig. 11. Experiment results of T_L switches from 0.02 Nm to $0.02 \sin(t)$ Nm under the fixed speed of 1500 r/min.

time (0.592 s) or maximum overshoot (129.71 r/min). Besides, compared with the GPC strategy, the proposed controller has a relatively smoother response curve, but slower regulation time, which causes by over strong robustness of the GPC method, i.e., unsurprisingly, the conservative horizon determination leads to a faster response time but a more intense process. The dynamic horizon converges from 1 s to 7.12 ms to 6.21 ms.

Scenario 2. The reference speed switches from 500 r/min to 3000 r/min with $T_L = 0.02$ Nm: Clearly, from Fig. 10, the phenomenon occurring to the PI controller is consistent with Scenario 1, i.e., longest settling time and largest overshoot. From the perspective of predictive control, one can find that the output speed behaviors of the GPC and GDPC are similar

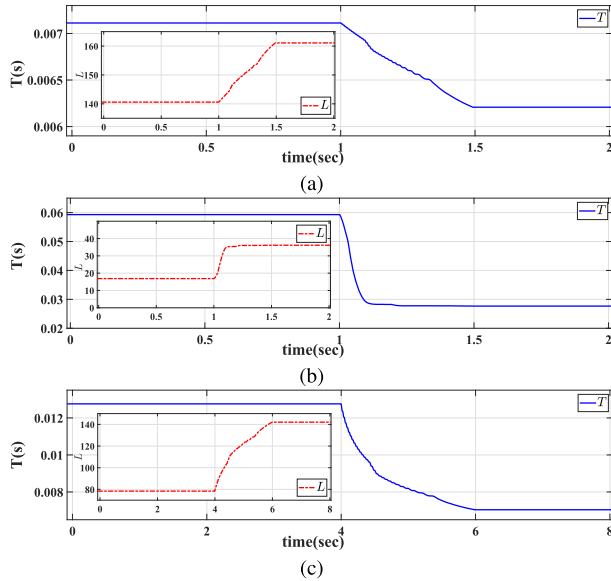


Fig. 12. Dynamic horizon response curves. (a) Scenario 1. (b) Scenario 2. (c) Scenario 3.

in this case. The philosophy of this manifestation is that the fixed horizon is artificially chosen as the most suitable value to confront this case (the worst case in these experiments), thereby the dynamic performance can be guaranteed. For the proposed dynamic horizon design, in this case, the dynamic horizon has to tune to the most conservative value (commonly close to the fixed horizon) according to the self-configuration mechanism, and only in this way can the sudden change of this severe working condition be suppressed, detailedly, and the dynamic horizon switches from 1 s to 59.31 ms to 27.68 ms.

Scenario 3. T_L switches from 0.02 Nm to $0.02 \sin(t)$ Nm with the fixed speed 1500 r/min: For this scenario, as shown in Fig. 11, the output response performance of all candidate controllers has a huge difference. First of all, the PI controller is unsatisfactory as always with the T_L presence of frequent switching, and the steady-state speed fluctuation seems to be hard to be accepted. The steady-state speed of the GDPC is relatively more desirable than the GPC, due to the horizon generated seems to be more suitable in this condition, which switches from 1s to 12.76 ms to 7.04 ms. At the T_L operation condition switching moment, the maximum overshoot of the conventional GPC is larger than the proposed GDPC, and the obvious speed fluctuation occurs in the PMSM drive system.

The detailed behavior data, integrated squared error (ISE) and mean squared error (MSE) of the candidate controllers are listed in Table III for reference. In summary, the controlled design expectancy of the proposed framework is basically achieved in the experimental verification.

VI. CONCLUSION

For the purpose of alleviating the optimization ability limitations of conventional MPC methods employing a fixed horizon in the presence of multiple working conditions, a novel GDPC synthesis scheme has been developed in this article. By this means, the horizon can realize autonomous, real-time

TABLE III
PERFORMANCE DATA OF ALL CANDIDATE CONTROLLERS (THE ISE AND MSE HAVE BEEN NORMALIZED)

Controller	Working condition	Maximum deviation/r/min	Settling time/s	ISE	MSE
The proposed controller	Case 1	0	0.543	0.845	0.845
	Case 2	0	0.68	0.927	0.927
	Case 3	15.32	/	0.010	0.010
The GPC strategy	Case 1	0	0.512	0.821	0.816
	Case 2	0	0.665	0.772	0.772
	Case 3	53.67	/	0.024	0.024
The PI controller	Case 1	129.71	0.592	1	1
	Case 2	343.16	0.726	1	1
	Case 3	98.13	/	1	1

adjustment according to the current operating conditions, and furthermore, the balance between robustness and adaptability is promisingly achieved. The control expectation is validated by both numerical simulation and application to the PMSM drive system. The output regulation theme for constrained systems will be further discussed in the future.

APPENDIX

To begin with, some essential lemmas are provided first for ease of understanding and derivation.

Lemma A.1: (Young's Inequality) If $p > 1$, $q > 1$, and $\frac{1}{p} + \frac{1}{q} = 1$, then $\forall a, b \geq 0$, the following inequality holds: $ab \leq \frac{q}{a^p} + \frac{b^q}{q}$.

Lemma A.2: (Barbalat's Lemma) If $\lim_{t \rightarrow \infty} g(t) < \infty$ exists, \dot{g} is uniformly continuous or \ddot{g} is bounded, then $\lim_{t \rightarrow \infty} \dot{g}(t) = 0$.

In what follows, the main stability proof for Theorem 3.1 is presented in detail.

Proof: Denote $e_{i,0} = \hat{x}_i - x_i$, $e_{i,j} = z_{i,j} - d_i^{(j-1)}$, $j = 1, 2, \dots, n-i$ and $N > 0$ as the boundness of d_i and its derivatives. Combining with Assumption 2 and the HOSMO (2), the error dynamics can be expressed as

$$\begin{aligned} \dot{e}_{i,0} &= e_{i,1} - \alpha_{i,0} l_i^{\beta_{i,0}} [e_{i,0}]^{1-\beta_{i,0}} \\ \dot{e}_{i,j} &= e_{i,j+1} - \alpha_{i,j} l_i^{\beta_{i,j}} [e_{i,j} - \dot{e}_{i,j-1}]^{1-\beta_{i,j}}, j = 1, \dots, n-i \\ \dot{e}_{i,n-i+1} &\in [-N, N] \\ &- \alpha_{i,n-i+1} l_i^{\beta_{i,n-i+1}} [e_{i,n-i+1} - \dot{e}_{i,n-i}]^{1-\beta_{i,n-i+1}}. \end{aligned} \quad (18)$$

From [30, Th. 5], one knows that for any possible well-defined trajectories $x(t)$, all signals in the error system (18) are uniformly bounded if the selection of l_i is proper, and there exists a finite-time instance $t_1 > 0$ such that $e_{i,j} = 0$, $t \in [t_1, \infty)$. On the basis of ensuring the convergence of the disturbance observer, the main semiglobal stability analysis of this article is presented as follows. To begin with, one can rewrite ξ -system as the following compact form:

$$\dot{\xi} = L(A - BK)\xi - (\varrho I_n + \Theta) \frac{\dot{L}}{L} \xi + F + \tilde{\varepsilon} \quad (19)$$

where $\xi \triangleq [\xi_1, \xi_2, \dots, \xi_n]^T$, $F \triangleq [F_1, F_2, \dots, F_n]^T$, $\tilde{\varepsilon} \triangleq [\tilde{\varepsilon}_1, \tilde{\varepsilon}_2, \dots, \tilde{\varepsilon}_n]^T$, $F_i = \frac{f_i(\bar{x}_i) - f_i(\bar{x}_i^{ref})}{L^{\varrho+i-1}}$, and $\tilde{\varepsilon}_i = \frac{\varepsilon_i}{L^{\varrho+i-1}}$, $i = 1, \dots, n$.

Construct a Lyapunov candidate function as $W(\xi) = \xi^\top Q \xi$, and one can get that $W(\xi) \leq \lambda_{\max}(Q) \|\xi\|^2$. According to [30] and *Assumption 2*, it is clear that the observer errors do not converge to zero in the initial period, i.e., there exists a bounded constant Γ satisfying $\sup_{i=1,2,\dots,n} \{|\varepsilon_i|\} \leq \Gamma$. Keeping these basic deductions in mind, the first few steps of the proof are presented in sequence.

Take the time derivative of $W(\xi)$ along system (19), i.e.,

$$\begin{aligned}\dot{W}(\xi) &= L \frac{\partial W(\xi)}{\partial \xi^\top} (A - Bk)\xi - \frac{\partial W(\xi)}{\partial \xi^\top} (\varrho I_n + \Theta) \frac{\dot{L}}{L} \xi \\ &\quad + \frac{\partial W(\xi)}{\partial \xi^\top} F + \frac{\partial W(\xi)}{\partial \xi^\top} \tilde{\varepsilon}.\end{aligned}\quad (20)$$

Similar to the estimations of (22) and (23) based on the mathematical scaling method in [29], we arrive at

$$L \frac{\partial W(\xi)}{\partial \xi^\top} (A - BK)\xi \leq -L \|\xi\|^2 \quad (21)$$

$$\frac{\partial W(\xi)}{\partial \xi^\top} F|_{\eta \in \Gamma_\eta} \leq \iota_1 \|\xi\|^2 \quad (22)$$

$$\frac{\partial W(\xi)}{\partial \xi^\top} (\varrho I_n + \Theta) \frac{\dot{L}}{L} \xi \geq \iota_2 \frac{\dot{L}}{L} \|\xi\|^2 \geq 0 \quad (23)$$

where Γ_η is an any given compact set, and the constant $\iota_1 > 0$ dependent on Γ_η . $\iota_2 = 2\varrho\lambda_{\min}(Q) + \lambda_{\min}(\Theta Q + Q\Theta) > 0$ is a constant.

Next, the stability analysis of $\tilde{\varepsilon}$ can be divided into the following two parts: 1) $t \in [0, t_1]$; 2) $t \in [t_1, \infty)$.

Case 1. $t \in [0, t_1]$: Using *Lemma A.1*, one can get that

$$\begin{aligned}\frac{\partial W(\xi)}{\partial \xi^\top} \tilde{\varepsilon} &\leq 2\lambda_{\max}(Q) \|\xi\| \|\tilde{\varepsilon}\| \leq 2\sqrt{n}\lambda_{\max}(Q) \|\xi\| \Gamma \\ &\leq \iota_3 \|\xi\|^2 + \Gamma^2\end{aligned}\quad (24)$$

where $\iota_3 = n\lambda_{\max}^2(Q)$.

Case 2. $t \in [t_1, \infty)$: In this time interval, it is obvious that $e_{i,j} = 0 \Rightarrow d_i^{(j)} = \widehat{d}_i^{(j)} \Rightarrow \varepsilon_i = 0$ for $i = 1, 2, \dots, n$, $j = 0, 1, \dots, n-i$.

A. Boundness of the Dynamic Horizon T

In this subsection, we shall present the explanation of the boundness of T . Notably, $\dot{L}(t)$ is a positive semidefinite function. Then, a prior hypothesis is set that $L(t)$ will escape at a finite time t_f , i.e., $\lim_{t \rightarrow t_f} L(t) = \infty$. For an arbitrary large set Γ_η , there exists a proper finite-time instant $t^* \in [0, t_f]$ such that $L(t^*) \geq \iota_1 + \iota_3 + 1$. Thereafter, substituting (21)–(24) into (20), we arrive at

$$\begin{aligned}\dot{W}(\xi)|_{\eta \in \Gamma_\eta} &\leq -(L - \iota_1 - \iota_3) \|\xi\|^2 + \Gamma^2 \\ &\leq -\lambda_{\max}^{-1}(Q) W(\xi) + \Gamma^2, \quad \forall t \in [t^*, t_f].\end{aligned}\quad (25)$$

Further, we consider the following relationship:

$$\begin{aligned}+\infty &= L(t_f) - L(t^*) = \int_{t^*}^{t_f} \dot{L} d\tau \leq c \int_{t^*}^{t_f} (-\dot{W} + \Gamma^2) d\tau \\ &= c(W(t^*) - W(t_f)) + c\Gamma^2(t_f - t^*) = \text{constant}.\end{aligned}\quad (26)$$

Hence, it is obvious that (26) leads to a contradiction. Then, it can be concluded that the self-tuning bandwidth factor L is bounded in $\forall t \geq 0$. And furthermore, for the adaptive horizon T , one can get that it will clearly converge to a certain value from the transformation $T = T_0/L$ and $T_0 > 0$.

B. Uniform Boundness of States

Thereafter, define a proper level set first. For any bounded $x(t) \in [-\rho, \rho]^n$, there exists a constant $\bar{\rho} > 0$ such that $\max_{i=1,2,\dots,n} \{\sup_{t \geq t^*} |x_i^{\text{ref}}(t)|\} \leq \bar{\rho}$. Subsequently, the level set can be defined as $\Omega \triangleq \{\eta \in \mathbb{R}^n | W(\eta) \leq W_{\max} \triangleq \sup_{\eta \in \mathcal{V}_\eta} \{\eta^\top Q \eta\}\}$, where $\mathcal{V}_\eta \triangleq [-(\rho + \bar{\rho}), (\rho + \bar{\rho})]^n$. In what follows, with the fact that $L \geq 1$ and rescaled transformation, a prior conclusion can be drawn that $\forall \eta(t) \in \Omega$, $\xi(t)$ will stay in Ω forever.

To proceed, assume that the above statement is not true, i.e., at least one trajectory of $\eta(t)$ will escape the level set Ω within a finite time. Thereafter, according to the finite-time escaping phenomenon, there must exist a time instant $t_2 \geq t_*$, such that

$$(\eta(t_2))^\top Q(\eta(t_2)) = W_{\max}, \quad \dot{W}(\xi(t_2)) > 0. \quad (27)$$

Then, for any tolerance σ_0 satisfying $\sigma_0 \in \left(\frac{4\Gamma^2}{\lambda_{\min}^{-1}(Q)}, \frac{W_{\max}}{2}\right)$, the following relationship holds:

$$\begin{aligned}\dot{W}(\xi(t_2))|_{\eta \in \Omega} &\leq -\|\xi(t_2)\|^2 + \Gamma^2 \\ &\leq -\lambda_{\max}^{-1}(Q)(W_{\max} - \frac{\sigma_0}{4}) < 0.\end{aligned}$$

Recalling relation (27) leads to an obvious contradiction. Then, one can conclude that $\forall x(0) \in [-\rho, \rho]^n \Rightarrow \eta \in \Omega \Rightarrow \xi \in \Omega, \forall t \geq 0$.

C. Asymptotic Convergence of States

Define $G \triangleq \int_{t^*}^t \|\xi\|^2 d\tau$. Then, the following relation holds:

$$\begin{aligned}\lim_{t \rightarrow \infty} G &\leq \int_{t_*}^{t_1} (\Gamma^2 - \dot{W}) dt - \int_{t_1}^{\infty} \dot{W} dt \\ &\leq W(t^*) + \Gamma^2(t_1 - t^*) < \infty.\end{aligned}$$

Hence, combined with (19), (22), and $\xi \in \Omega$, both $\dot{\xi}$ and $\tilde{G} = 2(\xi_1 \dot{\xi}_1 + \dots + \xi_n \dot{\xi}_n)$ are uniformly bounded. By *Lemma A.2*, $\lim_{t \rightarrow \infty} \tilde{G} = 0 \Leftrightarrow \lim_{t \rightarrow \infty} \xi = 0$, i.e., $\lim_{t \rightarrow \infty} y = y_r$ holds.

At this point, the proof of *Theorem 3.1* is completed. ■

REFERENCES

- [1] S. J. Qin and T. A. Badgwell, "A survey of industrial mode predictive control technology," *Control Eng. Pract.*, vol. 11, no. 7, pp. 733–764, 2003.
- [2] W-H. Chen, D. J. Ballance, and P. J. Gawthrop, "Optimal control of nonlinear systems: A predictive control approach," *Automatica*, vol. 39, pp. 633–641, 2003.
- [3] F. Wang, X. Mei, J. Rodríguez-gómez, and R. Kennel, "Model predictive control for electrical drive systems—an overview," *CES Trans. Elect. Machines System*, vol. 1, no. 1, pp. 219–230, 2017.
- [4] J. D. Barros, J. F. A. Silva, and E. G. A. Jesus, "Fast-predictive optimal control of NPC multilevel converters," *IEEE Trans. Ind. Electron.*, vol. 60, no. 2, pp. 619–627, Feb. 2013.
- [5] J. Yang, W. X. Zheng, S. Li, B. Wu, and M. Cheng, "Design of a prediction-accuracy-enhanced continuous-time MPC for disturbed systems via a disturbance observer," *IEEE Trans. Ind. Electron.*, vol. 62, no. 9, pp. 5807–5816, Sep. 2015.

- [6] A. Liu, W-A. Zhang, L. Yu, H. Yan, and R. Zhang, "Formation control of multiple mobile robots incorporating an extended state observer and distributed model predictive approach," *IEEE Trans. Syst. Man, Cybern.: Syst.*, vol. 50, no. 11, pp. 4587–4597, Nov. 2018.
- [7] S. Chai, L. Wang, and E. Rogers, "A cascade MPC control structure for a PMSM with speed ripple minimization," *IEEE Trans. Ind. Electron.*, vol. 60, no. 8, pp. 2978–2987, Aug. 2013.
- [8] E. Fuentes, C. A. Silva, and R. M. Kennel, "MPC implementation of a quasi-time-optimal speed control for a PMSM drive, with inner modulated-FS-MPC torque control," *IEEE Trans. Ind. Electron.*, vol. 63, no. 6, pp. 3897–3905, Jun. 2016.
- [9] H. Liu and S. Li, "Speed control for PMSM servo system using predictive functional control and extended state observer," *IEEE Trans. Ind. Electron.*, vol. 59, no. 2, pp. 1171–1183, Feb. 2012.
- [10] S. Li, J. Yang, W-H. Chen, and X. Chen, *Disturbance Observer-Based Control: Methods and Applications*. Boca Raton, FL, USA: CRC Press, 2014.
- [11] A. J. Schaft, " L_2 -gain analysis of nonlinear systems and nonlinear state-feedback H_∞ control," *IEEE Trans. Autom. Control*, vol. 37, no. 6, pp. 770–784, Jun. 1992.
- [12] J. Yang, S. Li, X. Chen, and Q. Li, "Disturbance rejection of dead-time processes using disturbance observer and model predictive control," *Chem. Eng. Res. Des.*, vol. 89, pp. 125–135, 2011.
- [13] W-H. Chen, J. Yang, L. Guo, and S. Li, "Disturbance-observer-based control and related methods-An overview," *IEEE Trans. Ind. Electron.*, vol. 63, no. 2, pp. 1083–1095, Feb. 2016.
- [14] J. Han, "From PID to active disturbance rejection control," *IEEE Trans. Ind. Electron.*, vol. 56, no. 3, pp. 900–906, Mar. 2009.
- [15] N. Gu, D. Wang, Z. Peng, J. Wang, and Q-L. Han, "Disturbance observers and extended state observers for marine vehicles: A survey," *Control Eng. Pract.*, vol. 123, pp. 105158, 2022.
- [16] Q. Deng, Y. Peng, D. Qu, T. Han, and X. Zhan, "Neuro-Adaptive Containment Control of Unmanned Surface Vehicles With Disturbance Observer and Collision-Free," *ISA Transactions*, vol. 129, Part A., pp. 150–156, 2022.
- [17] Y. Mahgoub and A. El-Badawy, "Nonlinear disturbance observer-based control of a structural dynamic model of a twin-tailed fighter aircraft," *Nonlinear Dyn.*, vol. 108, pp. 315–328, 2022.
- [18] X. K. Chen, S. Komada, and T. Fukuda, "Design of a nonlinear disturbance observer," *IEEE Trans. Ind. Electron.*, vol. 47, no. 2, pp. 429–437, Apr. 2000.
- [19] J. Back and H. Shim, "Adding robustness to nominal output-feedback controllers for uncertain nonlinear systems: A nonlinear version of disturbance observer," *Automatica*, vol. 44, no. 10, pp. 2528–2537, 2008.
- [20] L. Kong and J. Yuan, "Disturbance-observer-based fuzzy model predictive control for nonlinear processes with disturbances and input constraints," *ISA Trans.*, vol. 90, pp. 74–88, 2019.
- [21] A. Zamani and H. Bolandi, "Robust MPC for tracking changing setpoints in discrete-time non-linear systems with non-additive unknown disturbance," *IET Control Theory Appl.*, vol. 16, no. 9, pp. 846–860, 2022.
- [22] C. Liu, W-H. Chen, and J. Andrews, "Tracking control of small-scale helicopters using explicit nonlinear MPC augmented with disturbance observers," *Control Eng. Pract.*, vol. 20, no. 3, pp. 258–268, 2012.
- [23] H. Xie, L. Dai, Y. Lu, and Y. Xia, "Disturbance rejection MPC framework for input-affine nonlinear systems," *IEEE Trans. Autom. Control*, vol. 67, no. 12, pp. 6595–6610, Dec. 2022, doi: [10.1109/TAC.2021.3133376](https://doi.org/10.1109/TAC.2021.3133376).
- [24] J. Wang, L. Chen, and Q. Xu, "Disturbance estimation-based robust model predictive position tracking control for magnetic levitation system," *IEEE/ASME Trans. Mechatronics*, vol. 27, no. 1, pp. 81–92, Feb. 2022.
- [25] E. F. Camacho and C. Bordons, *Model Predictive Control*. Berlin, Germany: Springer, 2007.
- [26] J. Yang, H. Cui, S. Li, and A. Zolotas, "Optimized active disturbance rejection control for DC-DC buck converters with uncertainties using a reduced-order GPI observer," *IEEE Trans. Circuits Syst. I: Regular Papers*, vol. 65, no. 2, pp. 832–841, Feb. 2018.
- [27] X. Dong, C. Zhang, T. Yang, and J. Yang, "Nonsmooth dynamic tracking control for nonlinear systems with mismatched disturbances: Algorithm and practice," *IEEE Trans. Ind. Electron.*, vol. 70, no. 4, pp. 4048–4057, Apr. 2023.
- [28] H. Lei and W. Lin, "Universal adaptive control of nonlinear systems with unknown growth rate by output feedback," *Automatica*, vol. 42, no. 10, pp. 1783–1789, 2006.
- [29] C. Zhang, J. Yang, Y. Yan, L. Fridman, and S. Li, "Semiglobal finite-time trajectory tracking realization for disturbed nonlinear systems via higher-order sliding modes," *IEEE Trans. Autom. Control*, vol. 65, no. 5, pp. 2185–2191, May 2020.
- [30] A. Levant, "Higher-order sliding modes: Differentiation and output-feedback control," *Int. J. Control.*, vol. 76, no. 9, pp. 924–941, 2003.
- [31] Y. Yan, C. Zhang, A. Narayan, J. Yang, S. Li, and H. Yu, "Generalized dynamic predictive control for nonparametric uncertain systems with application to series elastic actuators," *IEEE Trans. Ind. Informat.*, vol. 14, no. 11, pp. 4829–4840, Nov. 2018.
- [32] D. Swaroop, J. K. Hedrick, P. P. Yip, and J. C. Gerdes, "Dynamic surface control for a class of nonlinear systems," *IEEE Trans. Autom. Control*, vol. 45, no. 10, pp. 1893–1899, Oct. 2000.
- [33] M. Chen, G. Tao, and B. Jiang, "Dynamic surface control using neural networks for a class of uncertain nonlinear systems with input saturation," *IEEE Trans. Neural Netw. Learn. Syst.*, vol. 26, no. 9, pp. 2086–2097, Sep. 2015.
- [34] C. Dai, T. Guo, J. Yang, and S. Li, "A disturbance observer-based current-constrained controller for speed regulation of PMSM systems subject to unmatched disturbances," *IEEE Trans. Ind. Electron.*, vol. 68, no. 1, pp. 767–775, Jan. 2021.



Xin Dong (Member, IEEE) received the B.Sc. degree from the Changxian College, Southeast University, Nanjing, China, and the M.Sc. degree from the College of Automation Engineering, Shanghai University of Electric Power, Shanghai, China, in 2019 and 2022, respectively, both in electrical engineering.

He is currently with the College of Automation Engineering, Shanghai University of Electric Power. His research interests include nonlinear system control theory and applications for dc microgrids and PMSM.

He is a Member of the Intelligent Autonomous Systems Laboratory.



Jianliang Mao (Member, IEEE) received the B.Sc., M.Sc., and Ph.D. degrees in control theory and control engineering from the School of Automation, Southeast University, Nanjing, in 2011, 2014, and 2018, respectively.

From 2018 to 2021, he was with the Research and Development Institute, Estun Automation Co., Ltd. He is currently with the College of Automation Engineering, Shanghai University of Electric Power, Shanghai, China. His research interests include MPC, SMC, and vision-based their applications to electric drives and robotic

interactive control and manipulators.



Yunda Yan (Member, IEEE) received the B.Sc. degree in automation and the Ph.D. degree in control theory and control engineering from the School of Automation, Southeast University, Nanjing, China, in 2013 and 2019, respectively.

From 2020 to 2022, he was a Research Associate with the Department of Aeronautical and Automotive Engineering, Loughborough University. In Dec 2022, he joined the School of Engineering and Sustainable Development, De Montfort University, Leicester, U.K., as a Lecturer in Control Engineering. His current research interest focuses on the safety-critical control design for autonomous systems, especially related to optimization and learning-based methods.



Chuanlin Zhang (Senior Member, IEEE) received the B.S. degree in mathematics and the Ph.D. degree in control theory and control engineering from the School of Automation, Southeast University, Nanjing, China, in 2008 and 2014, respectively.

From 2011 to 2012, he was a Visiting Ph.D. Student with the Department of Electrical and Computer Engineering, University of Texas at San Antonio, San Antonio, TX, USA. From 2016 to 2017, he was a Visiting Scholar with the Energy Research Institute, Nanyang Technological University, Singapore. Since 2014, he has been with the College of Automation Engineering, Shanghai University of Electric Power, Shanghai, China, where he is currently a Professor. His research interests include nonlinear system control theory and applications for power systems.



Jun Yang (Fellow, IEEE) received the B.Sc. degree in automation from the Department of Automatic Control, Northeastern University, Shenyang, China, and the Ph.D. degree in control theory and control engineering from the School of Automation, Southeast University, Nanjing, China, in 2006 and 2011, respectively.

Since 2020, he has been with the Department of Aeronautical and Automotive Engineering, Loughborough University, Loughborough, U.K., as a Senior Lecturer. His research interests include disturbance observer, motion control, visual servoing, nonlinear control, and autonomous systems.

Dr. Yang was the recipient of the EPSRC New Investigator Award. He serves as Associate Editor or Technical Editor for IEEE TRANSACTIONS ON INDUSTRIAL ELECTRONICS, IEEE-ASME TRANSACTIONS ON MECHATRONICS, IEEE Open Journal of Industrial Electronics Society, etc. He is a Fellow of IET.